ACS APPLIED MATERIALS & INTERFACES

RESEARCH ARTICLE

www.acsami.org

Chemically Treating Poly(3-hexylthiophene) Defects to Improve Bulk Heterojunction Photovoltaics

Ziqi Liang,* Matthew O. Reese, and Brian A. Gregg*

National Renewable Energy Laboratory, 1617 Cole Boulevard, Golden, Colorado 80401, United States

ABSTRACT:

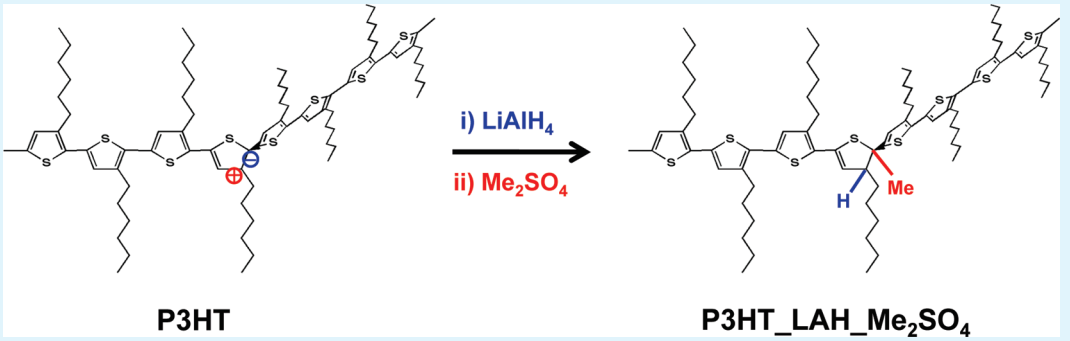

Defect engineering has been of vital importance to the development of inorganic semiconductors. Here, we report the chemical modification of electrical defects in the prototypical organic semiconductor, regioregular poly(3-hexylthiophene), P3HT. Previously, we have covalently treated defect sites with either a nucleophile or an electrophile, leaving the defects of primarily opposite polarity. Consecutively using both nucleophilic and electrophilic treatments allows us to covalently fix both positively and negatively charged defect sites in a single procedure. Here we describe the effects of treating P3HT first with lithium aluminum hydride, LAH, to decrease the overall defect density, and then with dimethylsulfate, Me_2SO_4, to eliminate some of the remaining n-type defects (equivalent to a p-type doping process). The resulting polymer, P3HT_LAH_Me_2SO_4, behaves differently than the polymer obtained when the order of treatments is reversed, P3HT_Me_2SO_4_LAH. Slightly improved structural and optical differences between these two new polymers and the starting P3HT are observed, whereas greatly improved electrical differences are found. Both treatments improve the performance of the photovoltaic cells, especially the short circuit current and the fill factor, and increase the stability against photodegradation. The significantly decreased series resistance and increased shunt resistance with a combined treatment suggest improved charge transport in the cell. The effective doping density can be increased or decreased with these treatments while the carrier mobility and the exciton diffusion length increase. It should be possible to employ these simple chemical treatments with any π-conjugated polymer to beneficially modify, or eliminate, some of its electronic defects. As a consequence, our approach provides a new method of improving the air-stability and electrical characteristics for organic photovoltaic and other electronic applications.

KEYWORDS: π-conjugated polymer, defect, chemical modification, organic photovoltaic cells

1. INTRODUCTION

The great promise of polymer-based photovoltaics[1−3] is that they can be manufactured in a low-cost, roll-to-roll manner on flexible substrates, just like photographic film. Many such organic photovoltaic (OPV) cells consist of a blend of π-conjugated polymers (π-CPs) as principal light absorber and electron donor with a soluble fullerene derivative (e.g., [6,6]phenyl-C61-butyric acid methyl ester, PCBM) as electron-acceptor in a bulk heterojunction (BHJ) structure.[4,5] Current power conversion efficiencies (η_p) of such cells are in the range of 6−8%.[6−11] The rapid increase in efficiency has somewhat outstripped our understanding of these materials which are far more complex than silicon. The highest-efficiency polymers are mostly based on donor−acceptor (D−A) alternating copolymers, which result in a lower bandgap (E_g) thereby harvesting more photons. The bandedges can be tuned via cautious structural design to attain a deep highest occupied molecular orbital (HOMO) energy level and hence better air-stability and also a higher open-circuit voltage (V_{oc}).[12−14] In addition, thermal[15−17] and solvent-vapor[18,19] annealing methods along with various chemical additives[20,21] are introduced in BHJ cells enabling the blend film to reach a both thermodynamically and kinetically optimum morphology, which enhances phase segregation and facilitates charge transport, leading to a higher η_p.[22,23] Because of the applied, and sometimes proprietary, nature of such work, and the rapid pace of new materials development, often little is known about the electronic and physical properties of these polymers.

The existence and influence of charged defects in organic semiconductors is not widely appreciated, yet they can have a

Received: March 4, 2011
Accepted: May 23, 2011
Published: May 23, 2011

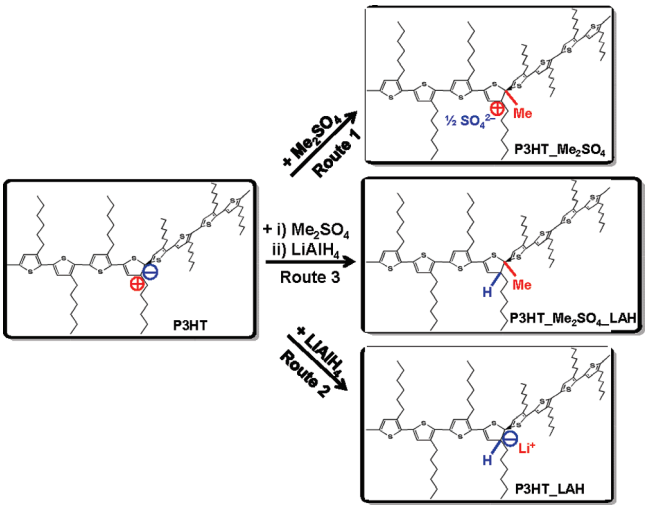

Figure 1. Possible reactions of hole and electron defects in P3HT with Me_2SO_4 (Route 1), LAH (Route 2), and Me_2SO_4 first and then LAH (Route 3), respectively. The addition of a hydride anion and a methyl cation can convert a strained and electroactive carbon−carbon double bond into a stable and electro-inactive carbon−carbon single bond.

powerful influence on the observed electrical and photovoltaic properties.[24−26] We recently demonstrated a defect engineering approach in regioregular poly(3-hexylthiophene), P3HT, a model polymeric semiconductor,[27−30] by employing electrophilic and nucleophilic reagents, e.g., Me_2SO_4 (dimethylsulfate) and LAH (lithium aluminum hydride), respectively.[31] Neither of these reagents are reactive enough to modify the unperturbed polymer, but they can react at defect sites where sp^2-hybridized carbons are distorted from their equilibrium positions and thereby destabilized. Removal of some defects (either hole or electron type) by nucleo- or electrophilic treatment enhances the P3HT photostability in air, suggesting that defects are a major source of chemical instability. Treatments also lead to enhanced exciton diffusion lengths and hole carrier mobilities. Free carrier densities, dark current activation energies, and Fermi energies can be adjusted either up or down by these treatments.[31] In those studies, one chemical reagent preferably reacts with a defect of one polarity, leaving the other defect of primarily opposite polarity, and the present work follows on to examine the effects of covalently modifying both defect sites (see Figure 1). Here we describe the effects of treating P3HT first with LAH to decrease the overall defect density, and then with dimethylsulfate, Me_2SO_4, to eliminate some of the remaining n-type defects (equivalent to a p-type doping process). The resulting polymer, P3HT_LAH_Me_2SO_4, is different than the polymer obtained when the order of treatments is reversed, P3HT_Me_2SO_4_LAH. Although significant changes have been previously observed in electronic performance of P3HT due to single treatments,[31] in this work, we also characterized microstructural changes of P3HT caused by either single or dual treatments since the film structure is known to strongly impact the electrical properties. The electronic changes after any treatment seem to result mainly from fewer charged defects but with a probable second-order influence from the slight structural variations observed in solid films. Finally, we choose the P3HT:PCBM BHJ cell,[32−34] a paradigm of OPV cells, to demonstrate how lower-defect P3HT interacts with PCBM in the blend and influences PV characteristics.

The approach employed here could be extended to modify any class of existing π-CPs, and improve their air stability and electrical characteristics for OPV applications. By contrast, current strategies to achieve such goals generally fall into one of two classes: synthesizing new materials or indirectly manipulating the film morphology through process control. For instance, the use of chemical additives improves the film morphology in BHJ cells and thus indirectly leads to enhanced charge transport by achieving better alignment of conjugated pathways between molecules. However, this method has followed an Edisonian approach and is not universally effective for every π-CP system. Our defect-engineering approach provides a new means, besides new synthesis and process control, to improve electrical transport in polymeric systems.

2. EXPERIMENTAL SECTION

Materials. P3HT and PCBM were obtained from Rieke Metals, Inc. (Item 4002-EE) and Nano-C, Inc. (Item nano-CPCBM-BF), respectively, and used as received. Note that the P3HT used at the start of these studies had the highest regioregularity available (i.e., ∼90−93%) at the time. For consistency, we continued to use the same P3HT in our subsequent studies. While over the course of this work higher regioregularity P3HT has become commercially available, it is not anticipated that the regioregularity difference will greatly affect the defect engineering process since we argue that the controlling factor is the removal of charged traps. All other chemical reagents and solvents were obtained from Aldrich and used without further purification.

Synthesis. All chemical reactions with P3HT were carried out under a N_2 atmosphere and the polymer was protected from light as much as possible. Yields from the reactions were 90% or more.

P3HT_Me_2SO_4 and P3HT_LAH. The syntheses were described in a previous report.[31]

P3HT_Me_2SO_4_LAH. To 80 mL of distilled tetrahydrofuran (THF) was added P3HT_Me_2SO_4 (250 mg), and the solution was stirred for 2 h. Seven millilters of 1 M lithium aluminum hydride (LAH) in THF was then added and allowed to react for 18 h at room temperature. Five milliliters of acetic acid was slowly added to quench the reaction followed by precipitation in 50 mL of methanol. After being stirred for 3 h, the precipitated polymer was filtered and washed with methanol. The product was dissolved in 30 mL of $CHCl_3$ and filtered through a 0.45 μm Teflon filter into 120 mL of methanol. The precipitate was filtered, washed with methanol, and dried in a vacuum desiccator.

P3HT_LAH_Me_2SO_4. To 100 mL of degassed anhydrous chlorobenzene, 400 mg of P3HT_LAH was added and stirred for 2 h. One milliliter of dimethylsulfate (Me_2SO_4, ***Caution**: this reagent is highly toxic!*) was added and the solution was stirred at room temperature for 18 h. Then 1 mL of triethylamine was added and stirred for 30 min before pouring slowly into 400 mL of stirring methanol. After 3 h, the precipitated polymer was filtered, washed with copious amounts of methanol and dried in a vacuum desiccator.

Film Preparation. Preparation of P3HT film samples was carried out in a N_2 atmosphere glovebox. P3HT (10−15 mg/mL) was dissolved in anhydrous chlorobenzene with heating and stirring overnight. Films were prepared by either spin-coating with a KW-4A spin-coater (Chemat Technology) or drop-casting on ITO-coated glass slides or Pt interdigitated electrodes (IDEs, AbTech Scientific). All P3HT films were then annealed at 130 °C for 15 min on a hot plate in the glovebox before the characterization and measurement. Film thickness was measured on an Alpha-step profilometer (Veeco Dektak 8 Advanced Development Profiler).

Characterization and Measurement. *Optical Properties.* Optical absorption spectra were recorded with an HP 8453 UV−vis

system. Fluorescence (FL) spectra were collected from 550−800 nm at 90° with respect to the excitation beam at ∼520 nm on a SPEX FluoroMax-4 spectrofluorometer (HORIBA JOBIN YVON, Inc., Edison, NJ). FL intensity was then normalized by absorbed photon numbers at the exciting light wavelength.

Thermal Analysis. Differential scanning calorimetry (DSC) experiments were measured on a TA Q1000 calorimeter under a N_2 atmosphere at a heating rate of 10 °C/min and a cooling rate of 5 °C/min in the temperature range of 40−300 °C. The first heating cycle was used to remove the thermal history. The total DSC curve has been corrected by subtracting a blank curve from the DSC signal. Sample size is ∼5 mg.

Diffraction Profiles. X-ray diffraction (XRD) studies were performed on a Scintag XGEN-4000 powder diffractometer equipped with a Cu Kα (1.54 Å) radiation source (40 kV, 40 mA) and a Scintag Peltier cooled solid-state detector. Drop-cast films were made onto $1'' \times 1''$ quartz substrates (Gem Dugout) cut 6° from (0001) that gave a low-background signal in the XRD measurement. Sample were mounted on a sample holder and scanned at 2θ ranging from 1.5 to 30° with a step size of 0.10°/min.

Dark Conductivity. Electrical conductivity was measured on Pt interdigitated electrodes (IDEs) with an electrode spacing of 10 μm. Polymer films were spin-coated on IDEs to a thickness approximately equal to the electrode height of 110 nm. Current−voltage ($I-V$) curves were acquired on a Keithley 236 Source Measure Unit by sweeping between −1 and +1 V with a step size of 0.01 V and a delay time of 100 ms.

Hole Mobility Measurement. Thick films for mobility measurements were prepared by solution casting of P3HT onto PEDOT:PSS-coated ITO glass slides and left to slowly evaporate overnight. Subsequently, Al electrodes were thermally evaporated onto the film. Current density−voltage ($J-V$) characteristics of the film were measured in the dark. The carrier extraction by linearly increasing voltage (CELIV) technique was used to measure hole mobility. A linearly increasing voltage pulse in reverse bias was applied with a function generator (Agilent 33220A). Current transients were monitored through a 50 Ω load on a Tektronix oscilloscope (DPO 7254, 2.5 GHz). RC constants were observed to be at least a factor of 1000 smaller than the time scales of interest.

Bulk Heterojunction Devices. Patterned indium tin oxide (ITO) substrates (12 Ω/square, Thin Film Devices, Inc.) were cleaned sequentially in ultrasonic solvent baths of acetone and isopropyl alcohol. After drying with a stream of N_2, the substrates were cleaned in an oxygen plasma (Technics 500-II Plasma System) for 5 min. The PEDOT-PSS (Baytron P VP AI 4083, now Clevios, resistivity ∼500−5000 Ω cm $=2 \times 10^{-4}$ to 2×10^{-3} S/cm) layer of ∼30 nm was spin-coated (Headway Research, Inc.) onto the ITO at 4000 rpm for 30 s and then baked on a hot plate at 120 °C for 60 min. Then the PEDOT-coated substrates were immediately transferred to a N_2-filled glovebox for preparing the active layer. A blend of P3HT:PCBM (1: 0.8 by weight) in anhydrous chlorobenzene with a total concentration of 18 mg/mL was spin-coated (Headway Research, Inc.) onto PEDOT:PSS-coated ITO glass slides at 400−600 rpm for 60 s, yielding the ∼150 nm thick active layer. The active layer was then annealed at 130 °C for 10 min. The samples were next loaded into a glovebox-integrated deposition chamber (Angstrom Engineering) and pumped down to a pressure of $<5 \times 10^{-8}$ Torr. A sequence of LiF (0.6 nm) and Al (100 nm) layers were sequentially deposited by thermal evaporation through a shadow mask at a rate of 0.1 and 2 Å/s, respectively. The shadow mask was used to define 6 pixels per superstrate where the active area is defined by the overlap of ITO anode and Al cathode as ∼0.11 cm^2. To avoid exposure to air, a vacuum-sealed container (TFS Technologies, KF40) was used during sample transfer from film coating to electrodes deposition and then device measurement in an inert atmosphere in a separate glovebox. The $J-V$ curves were measured with a Keithley 236 source−measure unit while illuminated with a homemade solar simulator at 100 mW/cm^2.[35] Solar-simulator illumination intensity was measured using a standard silicon photovoltaic with a KG filter (Hamamatsu S1787−04) calibrated by NREL's Measurement and Characterization group.

Film Topography. Topography of the P3HT:PCBM blend film on the PEDOT:PSS substrate was imaged with atomic force microscopy (AFM) in tapping mode on a Digital Instruments Dimension 3100 equipped with a Nanoscope IIIa controller. The height image was acquired at a scan rate of 1 Hz with a resolution of 256 × 256 pixels using a silicon etched tip (Nanotips, Veeco, Inc.) having a resonance frequency of ∼300 kHz and a spring constant of ∼40 N m^{1-}, and then processed using Nanoscope software version 6.1.3.

3. RESULTS AND DISCUSSION

Thin films of P3HT, and other π-CPs, have defect-rich regions that may dominate their electrical properties. Although not purposely doped, P3HT is, in fact, quite strongly doped p-type by its defects.[3,24,25] In physics terminology, this means that holes are "free," all free electrons have been annhilated, and the negative countercharges to the holes are trapped. In chemistry terminology, this means that some cations are delocalized while anions are localized. There must be equal numbers of the two to preserve charge neutrality. The charge density is expected to strongly affect the reactivity, thus, localized anions should be highly susceptible to attack by electrophiles such as Me_2SO_4, whereas delocalized cations may be less susceptible to attack by nucleophiles such as LAH. This might explain why Me_2SO_4 has a more pronounced effect on P3HT than LAH and even a combination of both Me_2SO_4 and LAH. But little is yet understood about the mechanistic details of these reactions: we can measure the resulting change in electrical and optical properties, but we do not yet know the actual chemistry because of the very small extent of reaction. This is a common problem in defect engineering of inorganic semiconductors: modifying defects that exist in the parts per million range can drastically alter the electrical properties of the semiconductor, yet the changes remain undetectable by normal chemical analysis.

We employed solution-phase reactions to treat P3HT with reagents such as LAH and Me_2SO_4.[31] One effect of these addition reactions is to rehybridize an electroactive sp^2 carbon to an electro-inactive sp^3 state. This not only removes a potentially electroactive defect in the solid state but it also creates flexible linkages along the polymer backbone. The flexible linkages can remove some of the inevitable morphological stresses in a polymer film without generating electroactive states in the bandgap. As-received P3HT was treated in solution by the two reagents in sequence. The order of the reaction sequence is given by the order of Me_2SO_4 and LAH in P3HT_Me_2SO_4_LAH and P3HT_LAH_Me_2SO_4. From our previous work,[31] we know that the LAH treatment by itself decreases the p-type defect density by ∼3 orders of magnitude. The Me_2SO_4 treatment by itself decreases the p-type defect density by 1 order of magnitude but the actual free hole density goes up because the remaining defects are shallower and a greater fraction of them is ionized. Figure 1 illustrates possible reactions in which a simplified defect in solid P3HT consisting of two full charges adjacent to each other undergoes chemical additions of LAH, Me_2SO_4, or both sequentially. The exact reactions taking place are not yet known. In conductivity measurements we have seen no evidence of mobile ions in the films (that is, $I-V$ sweeping in the dark is reversible, meaning a steady-state measurement); if they are present they must be electrostatically bound to their counterions, yet in the ppm scale. These types of defects are hypothesized to

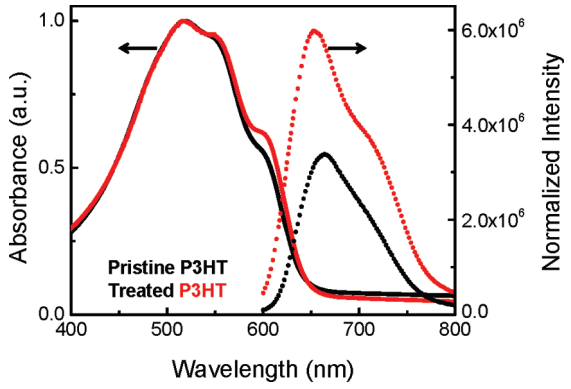

Figure 2. Representative comparison of UV−vis (solid line) and photoluminescence (dotted line) spectra of spun-coated P3HT films. Absorption data are normalized for comparison. Absorption spectrum of treated P3HT refers to P3HT_LAH_Me_2SO_4 and other treated samples' spectra are found between pristine P3HT and P3HT_LAH_Me_2SO_4. Emission data are corrected over absorption. Emission data of treated P3HT are acquired from averaging those of four treated samples.

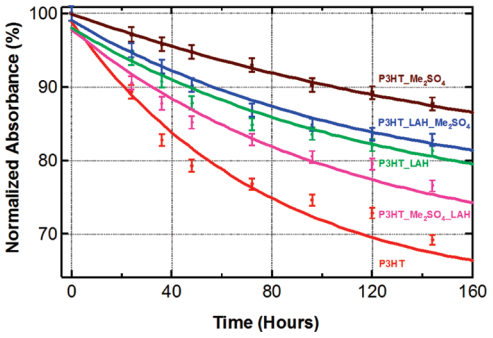

Figure 3. Temporal evolution of optical absorbance at 520 nm of P3HTs with and without chemical treatments when exposed to illumination in air.

also occur in solution, albeit transiently, at which point chemical reaction may occur. When the second treatment is performed, the reaction may modify what the previous reaction did or it may take place at a different site.

Optical Properties. Figure 2 compares solid-state optical spectra of pristine P3HT with those of treated P3HTs. The UV−vis absorption changes only slightly by treatment with either electrophile or nucleophile. The length of the chromophore should not change since apparently only ~1 in 10^4−10^5 of the polymer sites reacts.[36] All P3HT films show a maximum absorbance at ~520 nm, attributed to the π−π^* transitions along the conjugated backbone. The wavelength of maximum absorbance can vary depending on the spin-coating conditions and corresponding crystallinity of the film. Two vibronic shoulder peaks are found at ~550 and 610 nm due to intermolecular π−π stacking between thiophene rings. These two peaks are associated with P3HT aggregation as a result of thermal treatments. In the treated P3HT, the shoulder at ~610 nm becomes more pronounced, suggesting slightly increased ordering, presumably as a result of increased flexibility of less strained polymer chains. Photoluminescence (PL) spectra of all P3HT films display an identical main peak around ~670 nm, corresponding to the maximum absorption peak, yet the emission intensity of treated P3HT is significantly increased compared to pristine P3HT. These changes suggest that some defect sites that quench excitons have been removed. Excitons are known to be quenched by charged defects.[36] It was found that P3HT_Me_2SO_4 exhibits the highest emission intensity, approximately 3-fold higher than the untreated material. In addition, the shoulder at ~750 nm in the PL of treated P3HT, corresponding to the ~610 nm shoulder in the UV−vis, is appreciably enhanced.

Photo-oxidization Stability. The photostability of π-CPs in air is critically important for long-term applications. The photochemical stability was assessed by measuring the bleach times of P3HT films at their maximum optical absorbance under a white light illumination of ~18 mW/cm^2 by a tungsten bulb in air at room temperature with no active cooling.[31] Photobleaching studies (Figure 3) reveal the stability evolution against photo-oxidization in the following decreasing order: P3HT_Me_2SO_4 > P3HT_LAH_Me_2SO_4 > P3HT_LAH > P3HT_Me_2SO_4_LAH > P3HT. After illumination of a week (~160 h), P3HT_Me_2SO_4 shows the best stability, decreasing only about 13% of original absorbance, compared to a 33% loss in untreated P3HT. Among others, P3HT_LAH_Me_2SO_4 decreases 17%, about the same as that of P3HT_LAH (19%), whereas P3HT_Me_2SO_4_LAH losses 24%.

Thermal Transitions. Both the increased PL intensity and the enhanced photostability suggest that some nonradiative quenching pathways have been eliminated. DSC profiles of all P3HT bulk samples (Figure 4a and b) show a single peak for melting point (T_m) and temperature of crystallization (T_c), respectively. In general, we did not observe any side-chain melting and crystallization.[37,38] The glass transition temperature (T_g) is vaguely detectable. All the transition temperatures systematically decrease in the following order: P3HT_Me_2SO_4 (T_c = 200 °C, and T_m = 228 °C) > P3HT_LAH > P3HT_LAH_Me_2SO_4 ≅ P3HT_Me_2SO_4_LAH > P3HT (T_c = 194 °C, and T_m = 224 °C). The increased transition points of thermal phases (of a few degrees) in both exo- and endothermograms suggest that all treated P3HTs, although only a tiny portion of sites react, exhibit slightly denser intermolecular packing, from the increase in polymer flexibility around the treated sites, leading to slightly higher T_c and T_m. The modest changes in treated P3HTs are attributed to decreased covalent defect density along the conjugated backbone and the associated increased conformational flexibility that allows the polymer a better chance of finding a low energy conformation as the film dries. We believe that these modest changes will lead to an improvement, to a certain degree, in charge transport in films.

Structural Ordering. XRD patterns (Figure 5) of drop-cast P3HT films (~600 nm thick) all display primary (1 0 0), secondary (2 0 0) and tertiary (3 0 0) reflection peaks as expected, establishing the formation of highly regular lamellar structures.[30,39−42] We noted that these thick films have no changes in preferred orientation. These major diffraction peaks correspond to interlayer distances and follow the increasing trend at each 2θ position (i.e., decreasing lamellar d-spacing): P3HT_Me_2SO_4 < P3HT_Me_2SO_4_LAH < P3HT < P3HT_LAH_Me_2SO_4 < P3HT_LAH. Again, this modest change is likely due to the increased flexibility around the treated sites and may result in improved charge transport. We did not observe the (0 1 0) peak, corresponding to the π−π stacking of P3HT, in the 2θ range of 20−30°.

Conductivity, Mobility, and Carrier Density. The zero-field dark conductivity (σ, S/cm) was obtained from I−V curves on IDE substrates. The hole mobility data were acquired from the carrier extraction by linearly increasing voltage (CELIV) measurement. The time-of-flight (TOF) measurement is one of the

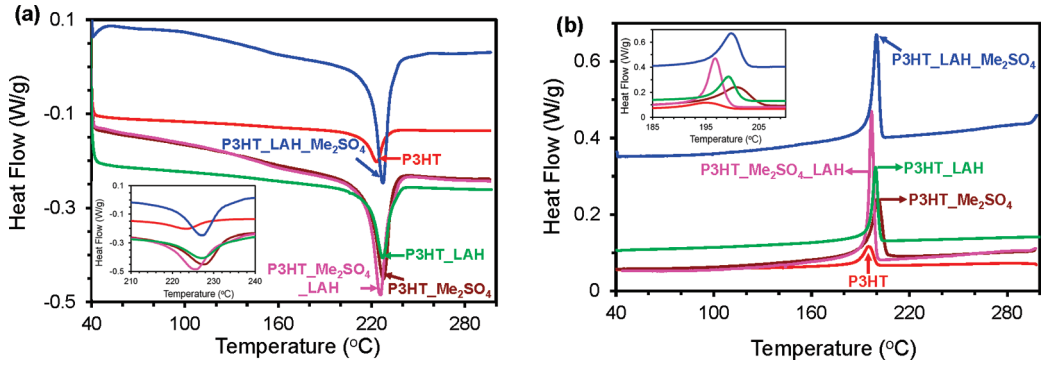

Figure 4. (a) DSC endotherm and (b) exotherm traces of all P3HT solid samples in the second heating cycle and the first cooling cycle, respectively. The inset magnifies the slight changes among the samples.

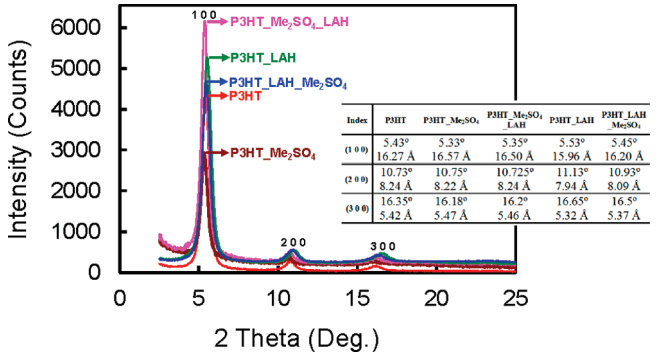

Figure 5. XRD diffractograms of drop-cast P3HT films on quartz substrates. Traces are offset slightly to clarify the peaks. Inset table shows 2θ and corresponding d-spacing values of diffraction peaks.

least ambiguous methods for estimating charge-carrier mobilities in bulk organic semiconductors, although it requires relatively thick films (>2 μm).[43,44] In contrast, CELIV was more recently developed and is more flexible with regard to film thickness.[45−47] Our previous reports support the consistency of CELIV with TOF measurements on P3HT.[31,36]

Hole mobilities are increased slightly by treatment with electrophiles (e.g., Me_2SO_4) and more substantially by treatment with nucleophiles (e.g., LAH).[31] This suggests that: i) the hole mobility is strongly affected by the defect density and that, ii) electron-rich defects, that is, those preferentially removed by electrophiles, are the most deleterious to hole transport. Here we measure hole mobilities via CELIV of P3HTs treated with both Me_2SO_4 and LAH as shown in Figure 6. The CELIV experiment was described previously.[31] The mobility data together with zero-field dark conductivity data are listed in Table 1. The two complementary treatments yield about the same electrical conductivity. But P3HT_LAH_Me_2SO_4 exhibits ~2× the hole mobility of P3HT_Me_2SO_4_LAH. The reason for the disparity may be related to either the better structural ordering (decreased lamellar spacing and increased higher-order peak intensity) or the lower value of the defect density and free hole density of P3HT_LAH_Me_2SO_4. It was anticipated that dual treatment would yield higher mobilities than either single treatment. In fact, this is true only for the Me_2SO_4 treatment, whereas the LAH treatment alone still yields the highest mobility yet achieved.

Thermal annealing of the P3HT:PCBM blend film is known to increase the crystallinity of P3HT phase and hence the hole mobility.[48] However, the change in hole mobility of pure P3HT is modest, for example, increasing from 1.7×10^{-4} to ~3.0×10^{-4} cm^2/(V s) upon film annealing at 180 °C, which corresponds to the crystallite size of P3HT increasing from 3.7 to 6.2 nm.[49] Improved charge transport in pure P3HT after annealing apparently occurs through reducing the number of amorphous interconnects between crystalline regions. However, because we observed much larger increases in hole mobility in both single[31] and dual treatments from starting P3HT, we believe these increases are unlikely to be caused by the slight structural improvement alone but rather mainly by a significant reduction in the charged trap density.

The dark conductivity is given by $\sigma(T,F) = q\, p_f(T,F)\, \mu_p(T,F)$ where q is the electronic charge, p_f is the free hole density (cm^{-3}), μ_p is the hole mobility (cm^2/(V s)), T is the temperature, and F is the applied electrical field (V/cm). As a result, the p_f of P3HT_Me_2SO_4_LAH is calculated as 2.5×10^{16} cm^{-3}, half that of pristine P3HT (5.3×10^{16} cm^{-3}),[31] whereas p_f of P3HT_LAH_Me_2SO_4 is ~80% lower than in pristine P3HT.

Photovoltaic Cell Characteristics. In view of the improved hole transport, we next investigate the photovoltaic performance of these low-defect P3HTs. We selected P3HT_LAH and P3HT_LAH-Me_2SO_4 for photovoltaic studies in a comparison with pristine P3HT as these two treated P3HTs exhibit the best hole-mobility and also allow us to compare the single to dual treatment. The BHJ device structure based on the P3HT:PCBM blend in a 1:0.8 weight ratio was used for comparison as it remains the best-performance configuration. We have previously used chlorobenzene (CB) as the solvent for preparing P3HT blend solution[31,36] and consequently CB continues to serve as the solvent in this study although the use of *o*-dichlorobenzene leads to improved efficiencies.[32] CB provides good solubility yielding nanosized phase separation of P3HT and PCBM. The mixed solution in CB was stirred at 60 °C for two days and then spin-coated on PEDOT:PSS modified ITO-glass slides, giving rise to 150 ± 10 nm in thickness for all samples. Because the films were all measured via profilometry (Veeco, Dektak 8) to be nominally the same thickness, a direct comparison of samples is possible. The film was subsequently annealed in a N_2 atmosphere at 130 °C for 10 min, followed by a sequential deposition of LiF and Al. Afterward, the device was measured both before and after a rapid annealing at 150 °C to ensure Ohmic contact between the electrodes and the active layer. A combination of LiF and Al offers stable electrodes, compared to Ca/Al in air, and better contact, compared to Al only.[35] The use of LiF instead of Ca also

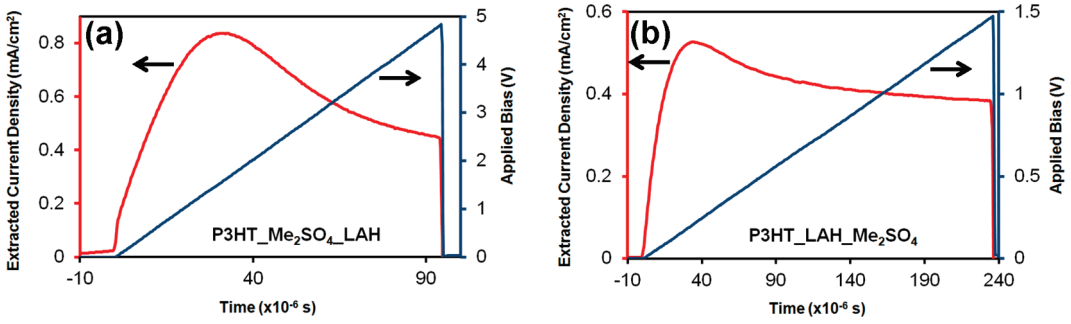

Figure 6. CELIV mobility measurements of P3HT treated with (a) Me_2SO_4 followed by LAH and (b) with the reverse order at an applied voltage ramp of 50 and 6 kV/s, respectively.

Table 1. List of Calculated Hole Mobility, Measured Dark Conductivity, And the Derived Free Hole Density from Figure 6[A]

polymer	dark conductivity (S/cm)	hole mobility ($cm^2/(V\,s)$)	free hole density (cm^{-3})
P3HT_Me_2SO_4_LAH	1.6×10^{-6}	4.0×10^{-4}	2.5×10^{16}
P3HT_LAH_Me_2SO_4	1.1×10^{-6}	7.2×10^{-4}	9.5×10^{15}
P3HT	1.2×10^{-6}	1.4×10^{-4}	5.3×10^{16}

[A] The data of starting P3HT are cited from ref 31.

avoids degrading the Ca during postannealing steps. The annealing of both film and device is a key for realizing a high-performance device, which benefits from the stronger absorption, the optimum surface morphology, and better metal contact obtained by the post-treatment. Figure 7 presents average photocurrent density−voltage bias ($J-V$) curves under AM 1.5G simulated solar irradiance and corresponding photovoltaic parameters with standard deviations reported in the inset table. Note that all data values plotted in $J-V$ curves represent an average of all six pixels on a single superstrate. All of these pixels show high dark rectification ratios (on the order of $\sim 1 \times 10^3$), suggesting improved shunt and series resistances by device annealing. Under illumination, the pristine P3HT:PCBM cell exhibits an average short-circuit current (J_{sc}), V_{oc}, and fill factor (FF) of 7.4 mA/cm^2, 583.5 mV and 59.8%, respectively, yielding an average η_p of 2.5 ± 0.1%. The measured efficiency is comparatively lower than the anomalously high efficiencies (5+%) sometimes seen in the literature reports using CB as solvent,[50,51] presumably because of the less conductive PEDOT:PSS we used.[52] It is, however, comparable to more carefully measured devices.[34] The cells composed of treated P3HT with LAH and LAH + Me_2SO_4 exhibit a η_p of 2.7 ± 0.1 and 3.2 ± 0.1%, respectively. These photovoltaic performance data are representative and reproducible from numerous samples under the same conditions, and the difference between these samples is unlikely from the sample variability.[35] The V_{oc} is limited by the difference in the energy levels of the electron donor and acceptor, that is, |HOMO (donor)−LUMO (acceptor)|, and by the carrier recombination rate. Nominally, our treatment should not affect the HOMO energy level of P3HT as it only alters the Fermi levels imparted by the doped state. There were, however, slight variations in V_{oc} (~2%) of a few standard deviations caused by the treatments. As opposed to pristine P3HT, P3HT_LAH lowers V_{oc} by 11 mV, whereas P3HT_LAH_Me_2SO_4 raises

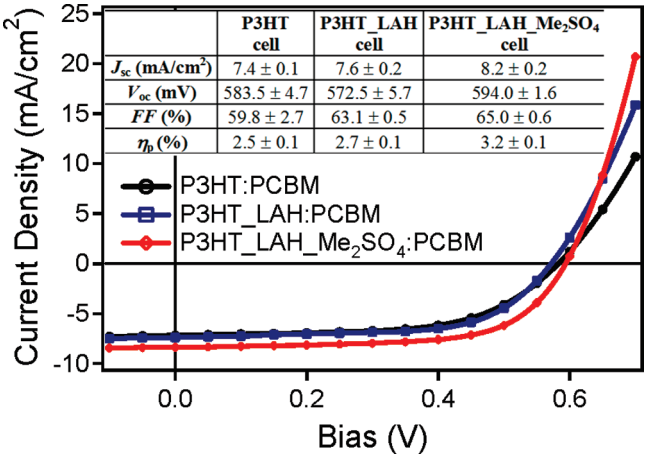

Figure 7. Average photocurrent density−voltage ($J-V$) characteristics of ITO/PEDOT:PSS/P3HT:PCBM/LiF/Al cells at a blend ratio of 1:0.8 by weight for pristine P3HT, P3HT_LAH, and P3HT_LAH_Me_2SO_4 with PCBM. The curves were measured at 100 mW/cm^2. All values plotted in $J-V$ are the average of six devices on one superstrate and listed in the inset table with the standard deviation.

V_{oc} by 10 mV with a much smaller standard deviation. This suggests that the treatments also slightly affect the recombination rate. The efficiency improvement occurs mostly from the increase in J_{sc} and FF. This may be partly due to increased hole mobility in which both treated P3HTs approach the electron mobility of PCBM which was reported as $\sim 2.0 \times 10^{-3}$ cm^2/V·s,[53] This results in a more balanced hole and electron transport within the BHJ network. Another factor in the improved efficiencies may be the longer exciton diffusion lengths in the treated samples.[31] It is important to note that the direction of the trends discussed were seen across several superstates for each treatment (the magnitude varied somewhat), although the data shown in Figure 7 is for averages of a representative single superstrate for each treatment rather than for best devices as often reported.

Of critical importance, the stability of BHJ devices using the treated P3HTs was also investigated. We showed previously that Me_2SO_4-treated P3HT-based BHJ cell with PCBM exhibits a substantial improvement in stability when the cells are processed in air, as compared to the performance of the untreated P3HT cell, which degrades substantially.[34] Here we investigated the long-term rate of degradation of unencapsulated devices with initial performance shown in Figure 7. The degradation

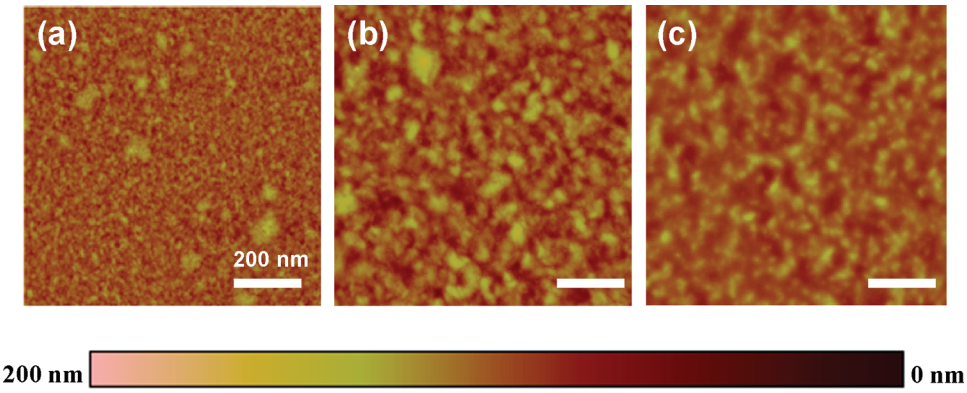

Figure 8. AFM height images of ITO/PEDOT:PSS/P3HT:PCBM films at a scan size of 1 × 1 μm: (a) untreated P3HT, (b) P3HT_LAH, and (c) P3HT_LAH_Me_2SO_4.

experiment was done over the course of a week with exposure to air and under continuous illumination.[54] A 5300 K sulfur plasma lamp (LG Electronics, PSH07) used for illumination, which was calculated to have a spectral mismatch factor of 1.002 (in relation to the devices and the KG filtered reference diode) and covers the wavelength range of UV−vis light with an onset around 400 nm and tailing off past 800 nm. The samples were aged in ambient relative humidity, which ranged from 20−30% with fluctuations in this range over the course of each day. The samples were actively cooled during illumination with chilled water, keeping their temperature near 25 °C. Over the first 10−20 h continuous illumination period, all the cells degraded similarly where the efficiency dropped by 40−60%. After this period, the treated samples degraded at a much slower rate (∼20% in 60 h) than one set of control devices (∼20% in 20 h). Unfortunately, a separate set of control devices also displayed enhanced stability, suggesting that the degradation process of this device architecture is quite complicated and even under similar processing and carefully controlled/similar aging conditions (temperature, relative humidity, illumination intensity and spectrum, load, and measurement interval) it is difficult to demonstrate definitively the enhanced photostability due to the treatments. We believe that this is due to the device architecture, which has many different pathways of degradation open to it, which obscure the enhanced photostability due to the treatments. These are likely due to a combination of factors including ITO etching/indium diffusion,[55] degradation of the PEDOT:PSS layer,[56] and photo-oxidation of the PCBM component resulting in deep level traps.[57]

Film Topography. A stable, nanophase-segregated morphology is required to achieve superior PV performance. Atomic force microscopy (AFM) in tapping-mode was used to characterize the surface topography of the active layers. Figure 8 shows representative topography profiles of P3HT:PCBM BHJ devices before deposition of the back electrode. All the films show a uniform and smooth morphology. Both treated P3HT-based BHJ films show comparable root-mean-square (r.m.s.) roughness to that of pristine P3HT. Compared to pristine P3HT, P3HT_LAH and P3HT_LAH_Me_2SO_4 based blend films show more distinct binary phase morphology with relatively bigger domains size. Slightly larger phase separation may assist charge extraction and reduce geminate recombination, helping to explain the difference in performance between pristine and treated devices. Yet the topographical difference between the two treated samples is small, making it difficult to explain their difference in device performance from surface morphology.

We note that photoinduced charge transfer occurs more efficiently in the following increasing order: P3HT < P3HT_LAH < P3HT_LAH_Me_2SO_4 in a 1:0.8 (by weight) blend with PCBM, based on PL quenching efficiency of P3HT, that is, 94 (in a good agreement with the literature),[58] 97, and 98%, respectively. Moreover, the improvement in transport is evidenced by the fact that the series resistance (R_s) decreases substantially from 412.7 Ω cm^2 in P3HT to 290.9 and 254.5 Ω cm^2 in P3HT_LAH and P3HT_LAH_Me_2SO_4, respectively, while the shunt resistance (R_{sh}) increases by ∼30% in P3HT_LAH and ∼40% in P3HT_LAH_Me_2SO_4. Lower R_s and higher R_{sh} suggest less intrinsic resistance and fewer defects which lead to reduced carrier recombination in the cell.[59] It is not clear yet whether the blend morphology of treated P3HTs films is beneficial, and therefore we believe that the enhanced charge transport in PV cells is largely due to improved electrical properties as a direct consequence of removing electronic defects or traps.

4. CONCLUSIONS

Treating P3HT with LAH, Me_2SO_4, or sequential combinations of the two, leads to improvements in fluorescence yield, exciton diffusion length, hole mobility, and polymer stability against photodegradation. The changes caused by the treatments are thought to be primarily due to the elimination of charged electrical defects, but also the slight changes observed in thermal properties and structural ordering are consistent with a slightly more flexible polymer chain leading to comparatively better packing. The p-type defect density (doping density) can be adjusted over several orders of magnitude by these treatments. The photovoltaic performance of bulk-heterojunction cells employing P3HTs treated with LAH, and sequentially with LAH followed by Me_2SO_4, yields more efficient cells than with the untreated P3HT. This is mainly due to an increase in J_{sc} and *FF*. The photodegradation is also slowed by these treatments. Such reactions with electrophiles and nucleophiles may be a general method for beneficially adjusting the electrical properties of any π-conjugated polymer. Of special note, our treatments may also improve the properties of organic field-effect transistors because these applications require well-ordered organic semiconductors having ambient stability, low defect density, and high carrier mobility.[60,61]

AUTHOR INFORMATION

Corresponding Author
*E-mail: ziqi.liang@nrel.gov (Z.L.); brian.gregg@nrel.gov (B.A.G.).

ACKNOWLEDGMENT

The authors thank Dr. Alex Hains for useful discussions. This work was funded by the U.S. Department of Energy, Office of Science, Basic Energy Science, Division of Chemical Sciences, Geosciences and Biosciences, under Contract DE-AC36-08GO28308 to NREL.

REFERENCES

(1) Shaheen, S. E.; Ginley, D. S.; Jabbour, G. E. *MRS Bull.* **2005**, *30*, 10–19.
(2) Brabec, C. J.; Durrant, J. R. *MRS Bull.* **2008**, *33*, 670–675.
(3) Hains, A. W.; Liang, Z.; Woodhouse, M. A.; Gregg, B. A. *Chem. Rev.* **2010**, *110*, 6689–6735.
(4) Yu, G.; Gao, J.; Hummelen, J. C.; Wudl, F.; Heeger, A. J. *Science* **1995**, *270*, 1789–1791.
(5) Halls, J. J. M.; Walsh, C. A.; Greenham, N. C.; Marseglia, E. A.; Friend, R. H.; Moratti, S. C.; Homes, A. B. *Nature* **1995**, *376*, 498–500.
(6) Park, S. H.; Roy, A.; Beaupré, S.; Cho, S.; Coates, N.; Moon, J. S.; Moses, D.; Leclerc, M.; Lee, K.; Heeger, A. J. *Nat. Photonics* **2009**, *3*, 297–303.
(7) Chen, H.-Y.; Hou, J.; Zhang, S.; Liang, Y.; Yang, G.; Yang, Y.; Yu, L.; Y., W.; Li, G. *Nat. Photonics* **2009**, *3*, 649–653.
(8) Liang, Y.; Xu, Z.; Xia, J.; Tsai, S.-T.; Wu, Y.; Li, G.; Ray, C.; Yu, L. *Adv. Mater.* **2010**, *22*, E135–E138.
(9) Price, S. C.; Stuart, A. C.; Yang, L.; Zhou, H.; You, W. *J. Am. Chem. Soc.* **2011**, *133*, 4625–4631.
(10) Zhou, H.; Yang, L.; Stuart, A. C.; Price, S. C.; Liu, S.; You, W. *Angew. Chem., Int. Ed.* **2011**, *50*, 2995–2998.
(11) http://www.forbes.com/feeds/businesswire/2010/07/27/businesswire142993163.html, accessed on July 27, 2010.
(12) Thompson, B. C.; Fréchet, J. M. J. *Angew. Chem., Int. Ed.* **2008**, *47*, 58–77.
(13) Chen, J.; Cao, Y. *Acc. Chem. Res.* **2009**, *42*, 1709–1718.
(14) Liang, Y.; Yu, L. *Acc. Chem. Res.* **2010**, *43*, 1227–1236.
(15) Camaioni, N.; Ridolfi, G.; Casalbore-Miceli, G.; Possamai, G.; Maggini, M. *Adv. Mater.* **2002**, *14*, 1735–1738.
(16) Padinger, F.; Rittberger, R. S.; Sariciftci, N. S. *Adv. Funct. Mater.* **2003**, *13*, 85–88.
(17) Savenije, T. J.; Kroeze, J. E.; Yang, X.; Loos, J. *Adv. Funct. Mater.* **2005**, *15*, 1260–1266.
(18) Li, G.; Yao, Y.; Yang, H.; Shrotriya, V.; Yang, G.; Yang, Y. *Adv. Funct. Mater.* **2007**, *17*, 1636–1644.
(19) Jo, J.; Na, S.-I.; Kim, S.-S.; Lee, T.-W.; Chung, Y.; Kang, S.-J.; Vak, D.; Kim, D.-Y. *Adv. Funct. Mater.* **2009**, *19*, 2398–2406.
(20) Peet, J.; Soci, C.; Coffin, R. C.; Nguyen, T. Q.; Mikhailovsky, A.; Moses, D.; Bazan, G. C. *Appl. Phys. Lett.* **2006**, *89*, 252105.
(21) Peet, J.; Kim, J. Y.; Coates, N. E.; Ma, W. L.; Moses, D.; Heeger, A. J.; Bazan, G. C. *Nat. Mater.* **2007**, *6*, 497–500.
(22) Moulé, A. J.; Meerholz, K. *Adv. Mater.* **2008**, *20*, 240–245.
(23) Bavel, S. v.; Sourty, E.; With, G. d.; Frolic, K.; Loos, J. *Macromolecules* **2009**, *42*, 7396–7403.
(24) Gregg, B. A. *Soft Matter* **2009**, *5*, 2985–2989.
(25) Gregg, B. A. *J. Phys. Chem. C* **2009**, *113*, 5899–5901.
(26) Liu, A.; Zhao, S.; Rim, S.-B.; Wu, L.; Könemann, M.; Erk, P.; Peumans, P. *Adv. Mater.* **2008**, *20*, 1065–1070.
(27) McCullough, R. D. *Adv. Mater.* **1998**, *10*, 93–116.
(28) Mao, H.; Xu, B.; Holdcroft, S. *Macromolecules* **1993**, *26*, 1163–1169.
(29) Bao, Z.; Dodabalapur, A.; Lovinger, A. J. *Appl. Phys. Lett.* **1996**, *69*, 4108–4110.
(30) Sirringhaus, H.; Brown, P. J.; Friend, R. H.; Nielsen, M. M.; Bechgaard, K.; Langeveld-Voss, B. M. W.; Spiering, A. J. H.; Janssen, R. A. J.; Meijer, E. W.; Herwig, P.; Leeuw, D. M. d. *Nature* **1999**, *401*, 685–688.
(31) Liang, Z.; Nardes, A.; Wang, D.; Berry, J. J.; Gregg, B. A. *Chem. Mater.* **2009**, *21*, 4914–4919.
(32) Li, G.; Shrotriya, V.; Huang, J.; Yao, Y.; Moriarty, T.; Emery, K.; Yang, Y. *Nat. Mater.* **2005**, *4*, 864–868.
(33) Kim, Y.; Cook, S.; Tuladhar, S. M.; Choulis, S. A.; Nelson, J.; Durrant, J. R.; Bradley, D. D. C.; Giles, M.; Mcculloch, I.; Ha, C.-S.; Ree, M. *Nat. Mater.* **2006**, *5*, 197–203.
(34) Bavel, S. S. v.; Bärenklau, M.; With, G. d.; Hoppe, H.; Loos, J. *Adv. Funct. Mater.* **2010**, *20*, 1458–1463.
(35) Reese, M. O.; White, M. S.; Rumbles, G.; Ginley, D. S.; Shaheen, S. E. *Appl. Phys. Lett.* **2008**, *92*, 053307.
(36) Wang, D.; Kopidakis, N.; Reese, M. O.; Gregg, B. A. *Chem. Mater.* **2008**, *20*, 6307–6309.
(37) Wu, Z.; Petzold, A.; Henze, T.; Thurn-Albrecht, T.; Lohwasser, R. H.; Sommer, M.; Thelakkat, M. *Macromolecules* **2010**, *43*, 4646–4653.
(38) Pascui, O. F.; Lohwasser, R.; Sommer, M.; Thelakkat, M.; Thurn-Albrecht, T.; Saalwächter, K. *Macromolecules* **2010**, *43*, 9401–9410.
(39) Kim, D. H.; Jang, Y.; Park, Y. D.; Cho, K. *Macromolecules* **2006**, *39*, 5843–5847.
(40) Kline, R. J.; DeLongchamp, D. M.; Fischer, D. A.; Lin, E. K.; Richter, L. J.; Chabinyc, M. L.; Toney, M. F.; Heeney, M.; McCulloch, I. *Macromolecules* **2007**, *40*, 7960–7965.
(41) Salleo, A.; Kline, R. J.; DeLongchamp, D. M.; Chabinyc, M. L. *Adv. Mater.* **2010**, *22*, 3812–3838.
(42) Yang, H.; Shin, T. J.; Yong, L.; Cho, K.; Ryu, C. Y.; Bao, Z. *Adv. Funct. Mater.* **2005**, *15*, 671–676.
(43) Van der Auweraer, M.; De Schryver, F. C.; Borsenberger, P. M.; Bässler, H. *Adv. Mater.* **1994**, *6*, 199–213.
(44) Chen, S.-G.; Stradins, P.; Gregg, B. A. *J. Phys. Chem. B* **2005**, *109*, 13451–13460.
(45) Juska, G.; Arlauskas, K.; Viliunas, M.; Genevicius, K.; Osterbacka, R.; Stubb, H. *Phys. Rev. B* **2000**, *62*, 16235.
(46) Mozer, A. J.; Sariciftci, N. S.; Lutsen, L.; Vanderzande, D.; Österbacka, R.; Westerling, M.; Juška, G. *Appl. Phys. Lett.* **2005**, *86*, 112104.
(47) Mozer, A. J.; Sariciftci, N. S.; Pivrikas, A.; Österbacka, R.; Juška, G.; Brassat, L.; Bässler, H. *Phys. Rev. B* **2005**, *71*, 035214.
(48) Mihailetchi, V. D.; Xie, H.; Boer, B. d.; Koster, L. J. A.; Blom, P. W. M. *Adv. Funct. Mater.* **2006**, *16*, 699–708.
(49) Flesch, H.-G.; Resel, R.; McNeill, C. R. *Org. Electron.* **2009**, *10*, 1549–1555.
(50) Ma, W.; Yang, C.; Gong, X.; Lee, K.; Heeger, A. J. *Adv. Funct. Mater.* **2005**, *15*, 1617–1622.
(51) Reyes-Reyes, M.; Kim, K.; Carroll, D. L. *Appl. Phys. Lett.* **2005**, *87*, 083506.
(52) Emery, K. A. *Appl. Phys. Lett.* **2007**, *91*, 266101.
(53) Mihailetchi, V. D.; Duren, J. K. v.; Blom, P. W. M.; Hummelen, J. C.; Janssen, R. A. J.; Kroon, J. M.; Rispens, M. T.; Verhees, W. J. H.; Wienk, M. M. *Adv. Funct. Mater.* **2003**, *13*, 43–46.
(54) Reese, M. O.; Morfa, A. J.; White, M. S.; Kopidakis, N.; Shaheen, S. E.; Rumbles, G.; Ginley, D. S. *Sol. Energy Mater Sol. Cells* **2008**, *92*, 746–752.
(55) Krebs, F. C.; Norman, K. *Prog. Photovoltaics* **2007**, *15*, 697–712.
(56) Kawano, K.; Pacios, R.; Poplavsky, D.; Nelson, J.; Bradley, D. D. C.; Durrant, J. R. *Sol. Energy Mater Sol. Cells* **2006**, *90*, 3520–3530.
(57) Reese, M. O.; Nardes, A. M.; Rupert, B. L.; Larsen, R. E.; Olson, D. C.; Lloyd, M. T.; Shaheen, S. E.; Ginley, D. S.; Rumbles, G.; Kopidakis, N. *Adv. Funct. Mater.* **2010**, *20*, 3476–3483.
(58) Piris, J.; Dykstra, T. E.; Bakulin, A. A.; Loosdrecht, P. H. M. v.; Knulst, W.; Trinh, M. T.; Schins, J. M.; Siebbeles, L. D. A. *J. Phys. Chem. C* **2009**, *113*, 14500–14506.

(59) Kim, M.-S.; Kim, B.-G.; Kim, J. *ACS Appl. Mater. Interfaces* **2009**, *1*, 1264–1269.
(60) Chabinyc, M. L.; Jimison, L. H.; Rivnay, J.; Salleo, A. *MRS Bull.* **2008**, *33*, 683–689.
(61) Arias, A. C.; MacKenzie, J. D.; McCulloch, I.; Rivnay, J.; Salleo, A. *Chem. Rev.* **2010**, *110*, 3–24.